Bottom Loss Measurements in a Spatially Variable Environment at the Sediment Acoustics Experiment 2004

Marcia J. Isakson, Nicholas P. Chotiros, and James N. Piper

Applied Research Laboratories,

The University of Texas at Austin,

Austin,

Texas 78713-8029 [a)]

H. John Camin

Applied Research Laboratory,

The Pennsylvania State University,

State College,

PA 16804

(Dated: October 5, 2010)

Abstract

Acoustic propagation in littoral environments is highly dependent on the reflection loss at the ocean bottom. In this study, bottom loss was measured over a nominally sandy sediment, as part of a larger program called "Sediment Acoustics Experiment 2004". Bottom loss was measured at grazing angles between 10 and 70 degrees and frequencies 10 to 50 kHz. The diversity in the measured loss indicated that the area was spatially variable with respect to sediment type. Reflections from mud, sand, gassy sediments and layered sediments were identifiable by parsing the data into statistically separable components that could be matched to known or inferred bottom loss models. This study indicates that in certain environments, predictive models require not only knowledge of the average sediment characteristics, but also the size and composition of sediment patches. The fact that a hurricane passed over the experiment site a week prior may have accentuated the heterogeneity.

PACS numbers: 43.30.Ma

I. INTRODUCTION

An understanding of the acoustic interaction at the ocean bottom is key to understanding propagation in littoral environments. One of the important features of this interaction is the reflection loss at the ocean bottom. However, it is difficult to accurately parameterize this value even in a spatially homogeneous environment as it is dependent not only on the type of ocean sediment but also the interface conditions including roughness, near interface gradients, and volume inhomogeneities. An ensemble of measurements taken over a spatially variable seabed will reflect the inhomogeneity. To properly analyze the data, they must be separated according to sediment type. Then, each type may be parameterized in terms of its properties and spatial statistics.

In this study, bottom loss measurements were conducted as part of the Sediment Acoustics Experiment 2004 (SAX04) which was conducted in the Gulf of Mexico near the Florida panhandle in September and October 2004. The test site was significantly perturbed by Hurricane Ivan which passed through one week before the measurements were taken and deposited a significant amount of non-local sediment. One goal of the study was to determine whether bottom loss measurements taken in this type of environment can be properly classified with regards to sediment type and to quantify its variability. Due to interface roughness, bottom loss often has the character of a random process. For a uniform bottom, it would be a stationary random process. The statistics of the measured bottom reflection loss at SAX04 showed that there was more than one random process, which indicated that the bottom consisted of patches of different bottom types. A parsing algorithm was developed to separate reflections from different sediment types and a classification of each type was performed based on known and inferred models. This work will be applicable in the parameterization of patchy bottoms in general. It will also aid in the development of methods to manage uncertainty in bottom loss for sonar performance modeling.

In this paper, a description of the experiment is presented in Sec. II. The data are

[a)]Electronic address: misakson@arlut.utexas.edu

analyzed and separated into statistically significant distributions in Sec. III. Models of the bottom loss are presented in Sec. IV. The data are classified and results are presented in Sec. V. Lastly, conclusions are drawn in Sec. VI.

II. EXPERIMENTAL SET-UP

Data were taken using a source mounted on a remotely operated vehicle and three receivers on a bottom-mounted vertical line array. The source was an ITC 1032 spherical transducer driven by a 1 ms linear chirp. Three different chirp wave forms were used with frequency bands from 4.5-10 kHz, 10-22 kHz and 22-50 kHz. Each frequency range required different matching impedance electronics for optimal projector efficiency. Switching between these three frequency ranges involved taking the projector out of the water and physically changing the source electronics. Each band was used on a different day in slightly different experimental conditions. The receivers were ITC 1089 omni-directional tranducers with a relatively flat response in the frequency range. Details of the source amplification and data acquisition system are described in a previous publication[1].

In order to localize the source relative to the receivers, an additional transducer was placed at the corner of the test site. A perspective view of the test site is shown in Fig. 1. The arrival times of the direct path signals through the water at all four receivers were used to determine the position of the source. Then the arrival time of the reflection was estimated based on a flat surface assumption. This estimate is used only to guide the algorithm in searching for the actual reflected path arrival. An example of a localization calculation is shown in Fig. 1. The length of the rays in the figure are determined by the arrival times. The sound speed profile was provided by the RV Seward Johnson through CTD measurements. The water column was isovelocity for all depths relevant to this experiment.

The source position was overdetermined since there are four arrival times for the three degrees of freedom of the source location. Three estimates of the source position were determined for each measurement. Pings in which the standard deviation of any source

position coordinate was above 10 cm were not considered. High variability in the source localization indicated a severe perturbation of the water column, for example, by a passing fish. The source was moved to many locations within the experimental area in order to include as many statistically independent reflections as possible.

The experiment was designed to cover the reflected angle range from 7-70 degrees grazing. Because of the severe turbidity from Hurricane Ivan, optical positioning was not possible and the vehicle generally remained on the sea floor for navigational purposes. Therefore the source was located nominally 0.5 m above the ocean floor for the duration of the experiment.

III. DATA ANALYSIS

The general data analysis method was described previously in Ref. 2. The procedure consists of four main steps: replica determination, direct path subtraction, grazing angle determination and bottom loss measurement.

A. Replica Determination

Unlike the laboratory procedure described in Ref. 2, a clean direct path replica without interference could not be obtained in situ. Replicas determined both pre- and post-experiment were inadequate for match filter since the in situ experimental set-up could not be recreated in the laboratory. This was mainly due to a mechanical coupling between the on site vertical line array and the receivers causing a change in the experimental transfer function and therefore the shape and frequency content of the received pulse. Therefore, a replica was determined from the measured data.

Since the source was close to the water/sediment interface, the direct path and reflected path arrivals overlapped in time. Therefore, the replica was determined by aligning the leading edge of the total signal and averaging. The reflected signals will decrease as $\sqrt{1/N}$ compared to the direct path signal since the arrival time of the reflected signal may be considered a random process. Here N is the number of independent ranges included in

the average. The source-receiver range varied from 0.5 to 4 meters giving a wide range of arrival times for the reflected path. Each data set was normalized to a 1 m source/receiver distance, correcting for spreading loss. An example of the alignment and averaging for the lowest frequency chirp is shown in Fig. 2. Fig. 2(a) shows the alignment on the first arrival. The average is the dark line. Fig. 2(b) shows the replicas determined for the three receivers for the lowest frequency signal. Note how the replicas are highly dependent on the particular receiver.

Many of the pings were not practical for use in replica determination for the lowest receiver because the direct path arrived before the receiver started recording. Therefore, there were few pings available for that receiver. Table I shows how many pings were included in the average for each chirp and receiver combination.

Although there were some differences in the transfer function among the receivers, there may have also been some contamination due to incomplete removal of the reflected signal. In order to quantify the effects of the residual reflected path, a simulation was conducted in which a replica was determined by averaging signals which included reflections from random ranges between 0.5 and 4 meters which encompasses the experimental range. The reflection coefficient was determined using the same method as for the measured data described below. For a low number of averages and in the low frequency band, the results can be extremely contaminated, more than 5 dB for less than 100 ping averages at 5 kHz. Therefore, the low frequency data will not be considered in this study. The average error for the higher frequency bands was below 2 dB.

B. Direct Path Subtraction

The replicas were aligned and subtracted from each ping to reveal the contribution of the non-direct path or paths. Shown in Fig. 3(a) is an example of the raw data and the data with direct path subtracted. Fig. 3(b) shows the matched filter response of the raw data, the direct path replica and the direct path subtracted data. This data represents the absolute

value of the raw time series match filtered with the empirical, receiver-dependent replica. The expected arrival time of the specularly reflected path based on the geometry and a flat interface assumption is also indicated by the solid black line. After direct path subtraction, much of the data exhibited more than one discrete peak as shown in Fig. 3(b). Each peak is consisdered to represent a discrete arrival. The two loudest arrivals were recorded for processing.

C. Grazing Angle and Depth of Reflection Determination

The estimated grazing angle and reflector depth for each measurement was determined from the known receiver geometry, calculated source position, time of arrival of the reflected path and an assumption of specular reflection from a horizontal reflecting surface. No a priori assumption was made for the depth of the seabed although an estimate of the nominal seabed depth based on the distance from the source to the seabed was used to guide the peak picking algorithm. The reflector depth as a function of source-receiver range is shown in Fig. 4. Here z=0 corresponds to the nominal seafloor level. Negative values indicate reflections from below the nominal seafloor. Only reflected arrivals within 1 meter of the nominal seabed depth are considered for analysis. Most of the data were within 15 cm of the nominal seabed. In the figure, some distinct layers are evident at the highest frequency range. These layers are mostly unresolved at lower frequencies.

D. Bottom Loss Measurement

The bottom loss was determined by the ratio of the peak of the matched filter response of the reflected path to the peak of the matched filter response of the direct path, correcting for spreading loss by using the ranges determined by arrival times. By normalizing the data by the direct path, the transducer response is effectively removed from the data. In addition, because the source was close to the seabed, the direct and reflected rays had very similar launch and arrival angles which lessens the impact of any imperfections in the nominally

omni-directional beam pattern of the transducers.

E. Sediment Variability

1. Depth of Reflection

In the high frequency (22-50 kHz) data, a layer is evident between 2.5 and 5 m range at a depth of 10 cm above the nominal seafloor. (See Fig. 4.) This suggests that data corresponding to depths significantly different from the nominal seafloor may constitute a fundamentally different process. For example, these data may correspond to scattering from fish near the seafloor. Therefore, before further analysis, the data is divided into three categories: near seafloor reflection defined as within 8 cm of nominal seafloor, shallow reflection defined as greater than 8 cm above the interface and deep reflection defined as greater than 8 cm below the interface. These data will be considered separately in further analysis.

2. Distribution Parsing

The data were taken from a sediment with known spatial variability. A visual inspection of the experimental area revealed mud patches interspersed with sand. Also, mud was prevalent in the area both on the surface and in flasers, laminae and depositional log layers as revealed by CT scans[3]. Therefore, the data must be separated into statistically significant regimes corresponding to reflection from the different sediments in the area. The data were binned by frequency and angle. The underlying distribution of the bottom loss for each sediment is likely to be Rician since it includes coherent (specular) and incoherent (scattered) components. If the coherent signal is large compared to the noise component, the Rician distribution can be approximated by a Gaussian in dB space. Therefore, for each frequency and angle bin, the data can be conveniently modeled as a superposition of Gaussian components and a parsing process to separate the different components was developed.

Before parsing, the data were compared to a single Gaussian distribution by means of the Kolmogorov-Smirnov test[4]. Only data which had less than a 10% probability of belonging to a single Gaussian distribution were considered for parsing. The parsing process consisted of the following steps. The distribution was first smoothed using a ten point boxcar filter. Peaks are identified using the first derivative. At each detected peak, a rough estimate of the amplitude, location and width of the Gaussian component was made. An iterative optimization process is used to refine the estimate by minimizing the difference between the sum of Gaussians and the measured histogram. An example of a parsed histogram is shown in Fig. 5. Note how the distributions have widths which are significantly less that 5.6 dB, the width of a Rayleigh-like process. This indicates that the distributions are Rician and can be estimated as Gaussians. Only significant Gaussian components with magnitudes over 5 counts were accepted.

IV. SEDIMENT MODELS

Using the method described in Section III, the center value and width of the parsed Gaussians were determined for each measured angle and frequency bin. The results are shown in Fig. 7 for two frequencies, each corresponding to a different chirp. The widths of the Gaussians are not included for clarity. The next step is to classify the type of sediment for each part of the data. For that, models of the different possible sediments are considered based on the measured parameters on site. Four types of sediment are considered sand, mud, gassy sediments or fish and layered sediments.

In order to describe bottom loss from sediments, three contributions are considered: reflection loss from a flat sediment interface, spherical wave effects, and interface scattering. The flat interface reflection loss generally describes the shape of the bottom loss curve as a function of angle and to a lesser extent, frequency since the attenuation is frequency dependent. The critical angle is dependent on the value of the sediment sound speed relative to the water sound speed and the normal incidence reflection is dependent on the impedance

mismatch of the sediment and the water.

Spherical wave effects occur when a spherical wave encounters a plane boundary. The plane wave components of the wave can be transmitted into the sediment at all angles. These refracted components travel in the sediment, reradiate into the upper layer evanescently and interfere with the specular reflection. For small geometries or low frequencies, these can modify the apparent critical angle and cause interference subcritically[2]. In these models, spherical wave effects are included naturally using the wave number integration technique using the Ocean Acoustics and Seismic Exploration Synthesis (OASES) modeling code developed at MIT[5]. Since spherical wave effects are highly dependent on the experimental geometry, the source-receiver geometry is modeled for each angle. The transfer function for the particular geometry is computed over the frequency range and a narrow band impulse response is computed using Fourier synthesis which is then processed using the same algorithm as the experimental data.

Lastly, interface scattering was considered. Unfortunately, the properties of the interface roughness at the test site were not measured due to extremely poor visibility. However, a coarse visual inspection revealed there were no well defined periodic structures such as ripples and the roughness appeared isotropic. This does not preclude a large scale ripple structure which may have been obscured by the overlying mud. Fortunately, the interface roughness was measured at other areas in the general vicinity. Therefore, these measurements will be used as the basis for an interface scattering analysis of the acoustic measurements. One such measurement was taken using a sediment conductivity probe, the IMP2[6]. The measured roughness can be described by a power-law fit to the measured power spectrum described by the following equation:

$$W(K) = \frac{w_1}{(K_L^2 + K^2)^{\gamma/2}} \tag{1}$$

Through a least-squares fit to the data, Tang et al specify the parameters as $w_1 = 0.0061$ $\text{cm}^{3-\gamma}$ and $\gamma = 2.82$. An examination of the roughness data also reveals that $K_L = 0.1$ cm^{-1} produces a good fit.

Realizations of the surface were produced from this power law spectrum according to the technique described in Ref. 7 and then used in a finite element model to determine the effects of scattering from the isotropic roughness on the measured forward scattered pressure. This method has been shown to agree well with the wavenumber integral method and to be more accurate over a larger range of roughness parameters than the Kirchhoff approximation or perturbation theory[8]. A full description of the finite element model used is beyond the scope of this paper although a short description is included below. Interested readers are directed to Ref. 8.

The finite element model was a three dimensional axially symmetric model with a point source placed at the origin. The commercial code, COMSOL, was used to mesh and solve the problem. The domain was truncated using perfectly matched layers. The scalings are described by Eqs. (33)-(35) in Ref. 9. The rough sand/water interface was 0.5 m below the source and the pressure is calculated at discrete points in the domain in order to model the range of angles. Time harmonic solutions to the Helmholtz equation at 250 Hz intervals between 24.5 and 30 kHz were calculated at these points and a time series was constructed through Fourier synthesis The resulting time series was analyzed using the same method as used for the experimental data as described in Section II. The Fourier synthesis method is more robust than purely time harmonic solutions since it includes finite bandwidth effects. By using a point source, the model intrinsically included spherical wave effects.

It was found that the scattering had little effect on the model at these frequencies relative to the variability in the data as shown in Fig. 6. Since scattering is a minor effect relative to the spatial variability, it will not be included in the further analysis.

3. Sand Reflections

Historically, the reflection loss for sands has been modeled using an elastic solid approximation. Recently, however, sound speed measurements have revealed dispersion which suggests that the elastic model is insufficient to model the interaction[10]. Newer models take

into account both the movement of the water and the movement of the sediment grains instead of considering sediments as an uniform solid. These models are referred to as poro-elastic models. The most accepted poro-elastic model is the Biot model[11,12] reformulated by Stoll[13] which is a two phase model that considers both the motion of the grains and the water with some inertial coupling and deviations from ideal flow at high frequencies. Current models attempt to account for differences between the predictions of the Biot/Stoll theory and observed dispersion and attenuation measurements[14,15,16].

The large uncertainties in the measurements due to sediment variability preclude discrimination between the fluid model and the more complex elastic or poro-elastic representations. Therefore, the simplest model, a fluid model, is used to model the reflection loss for sands. The data is compared to a reflection loss based on coarse sand since it was the most prevalent sediment in the area. The parameters were determined as follows. The water sound speed, density and attenuation are based on daily CTD measurements and tabular data[17]. The sand density is based on on-site measurements[18]. The sand sound speed and attenuation was measured on site[19]. These measurements were made at 400 kHz which is much higher than the measured frequencies. The parameters are summarized in Table II.

A. Mud Reflections

Reflection loss from muds is described in the same manner as that of sands. The main difference between the mud and sand models are the sediment parameters.

The mud density is determined from porosity measurements made by Briggs and Richardson[18] and Wheatcroft[20] who measured the porosity between 0.7 and 0.9. The mud sound speed is determined from the upper most layer of the measured mud sound speed reported by Briggs and Richardson[18]. The attenuation of mud is determined by empirical relationship between porosity and attenuation by Hamilton[21].

B. Gassy Sand Reflection

The observed reflection loss at angles between 50 and 60 degrees suggest that a patch of gassy sediment may have been in the area. For a model of the gassy sediment, both sand and mud models will fit the data since the effects of the gas dominate all structural properties of the sediment. The gassy sediment was modeled using a much lower density and sound speed as indicated in Table II. This analysis is applicable for any gas bearing material near the ocean floor including fish swim bladders.

C. Layered Reflections

In the general area of the experiment, mud layers and inclusions were common[3]. Therefore, models based on similar mud/sand layers are calculated and compared with the data. The models are computed with the OASP of OASES modeling code using the parameters in Table II. Models of sand in layers of 1 and 4 cm over a mud half-space were computed and compared with the data.

V. RESULTS

The data are compared with the models in Fig. 7 for both the lower frequency data centered at 16 kHz (Fig. 7(a)) and the higher frequency data centered at 32 kHz (Fig. 7(b)). The data were also categorized into sediment classes based on the least square error in dB. (The mean square error in linear units produced the same results.) The data are presented as the same color as the model to which they correspond. Note that for the lower frequency data, a small layer of mud over the sand has very little effect on the modeled bottom loss while at the higher frequency a resonance for that layer depth causes a large decrease in reflectivity relative to the sand case. Likewise, small changes in layer depths can cause large changes in reflectivity particularly near normal incidence.

Consider the higher frequency data relative to the models. Much of the data corresponds to a reflection from mud. This is especially the case for the deeper measurements suggesting

that the mud may be residing in lower lying areas. The reflections from near the interface were mostly sand or sand layers. Lastly, reflections from above the interface corresponded to gassy sediments or fish scattering particularly at higher grazing angles. This is consistent with fish swimming just above the seafloor.

The lower frequency data is less distinct. Some of the data lies between models. Note especially the sub-critical measurements. One of the reasons this data is less distinct is that the Fresnel zone of the interaction is larger, therefore it is more difficult to spatially resolve the sediment patches. The Fresnel zone for the 16 kHz reflection is approximately twice the size of that of the higher frequency. Also, the Fresnel zone for the lowest receiver, corresponding to the shallowest angles, is more than ten times the size of the two higher receivers. Therefore, sediment patches for low grazing angles are less likely to be resolved.

The variability of the sediment was calculated by considering the classification and the amplitude of the parsed distributions. For the purposes of this calculation, the data is classified according to the overlying sediment. For a center frequency of 36 kHz, 10% of the data corresponded to gassy sediments or fish, 59% of the data corresponded to mud and 31% of the data corresponded to either a half-space of sand or sand over a mud inclusion. For a center frequency of 16 kHz, 10% of the data corresponded to gassy sand or fish, 30% from mud, and 60% from sand. The difference in the measured variability between the two frequency ranges has two possible explanations. First, the measurements were taken on different days and may have probed both spatially and temporally different sediments. Currents in the area were still redepositing the sediment dynamically. Also, as explained above, the lower frequency measurements were not able to resolve the smaller sediment patches. Therefore, for smaller patches, the measured reflectivity would constitute an effective reflection from a mixture of mud and sand resulting in an incorrect classification.

A. Layered and Gassy Sediments Ambiguity

Many of the shallow measurements corresponded to what was classified as a "gassy sediment". There is some ambiguity between a gassy sediment and a layered sediment. Note how the lower frequency 4 cm sand over mud layer predicts values for bottom loss nearly the same as that of the gassy sediment. One method of distinguishing these processes is to consider the phase. For a layered sediment, a high value of reflectivity can be measured due to an incomplete resolution of the reflections from both the layers. In this case, the measured phase would be influenced by both reflections. The measurement would be random since the arrivals from the layers are not correlated if the layer depth is varying within a fraction of wavelength (11 cm at 16 kHz). However, if the reflection is due to a gassy sediment, the phase shift would be 180 degrees with very little spread.

A histogram of the measured phase response for reflection values greater than -6 dB between the grazing angles of 40 and 80 degrees is shown in Fig. 8. The wider angle range is included because there is evidence of a high reflectivity in the distributions for all of these angles. These reflections often do not meet the parsing criteria because there are very few of them. For example for 68 degrees grazing in Fig. 5, there is a small peak at -5 dB. This peak does not have an amplitude of 5 counts or more so it is not parsed.

Since the distribution of the phase shift for these returns is very consistent and almost exclusively 180 degrees, they are most likely from a gassy sediment. However, an alternate explanation may be scattering from biologics. For example, a small fish school or large single fish with a swim bladder in the area could also explain the phase shift. Additionally, these reflections were largely localized and almost exclusively above the nominal sea floor. In the area, there were some reflections from other sediments suggesting the phenomena may be dynamic. This also points to reflection from fish.

VI. CONCLUSION

Ocean bottom loss was measured for frequencies between 5 and 50 kHz at grazing angles between 10 and 70 degrees using a bottom-mounted three transducer vertical line array and a source mounted on an remotely operated vehicle. The data were analyzed by taking the ratio of the peaks of the match filter response of the reflected path to the direct path. Three frequency bands were used. The measurements from the lowest frequency band were found to be contaminated and were not considered. Using the measurements from the remaining two frequency bands, it was found that the bottom loss was inconsistent with a single stationary random process. Therefore, it was deduced that there was more than one sediment type, and that the bottom was a patch work of different sediment types.

The patchy bottom necessitated the use of statistical methods to isolate the component processes. The method chosen consisted of an algorithm to parse the measured histograms into stationary components. Each component was approximated by a Gaussian distribution in dB space. Three types of reflection interfaces were identified: water-sand, water-gassy sand or water/fish scattering, and water-mud. In addition, the spread of the data suggested that there may have been some layering of mud and sand.

The bottom loss was modeled based on the reflection loss from a flat sediment interface, spherical wave effects and scattering from the rough interface. The reflection loss was estimated using a fluid model approximation. Spherical wave effects were accounted for by modeling the data using wavenumber integration. Rough interface scattering was modeled using a finite element method, but was found to be insignificant with respect to the spread in the data.

The data were separated into three regimes based on the reflector depth and classified based on a least square error difference from the model. Reflections from near the interface were most often from sand. Reflections from lower lying areas were found to be consistent with scattering from mud while reflections from areas significantly above the nominal seafloor were consistent with scattering from a gassy sediment or fish swim bladders.

The methods developed will be applicable in the parameterization of patchy bottoms generally, and in the development of methods to manage uncertainty in bottom loss for sonar performance modeling. The data demonstrate that in spatially variant or 'patchy' environments, sediment variability has a large effect on the measured value of the bottom loss. However, using a Gaussian parsing method, the data can be classified as reflections from different sediments. For example, in this data set, after parsing the mud and sand reflections were clearly identified. In these environments, predictive models require not only knowledge of the sediment characteristics, but also the size and composition of sediment patches.

Acknowledgment

The authors would like to thank Eric Thorsos, the chief scientist of SAX04 and all of the participants for their contributions. Special thanks to Kevin Briggs and the NRL dive team for their support with environmental measurements. Thanks to the crew of the R/V Seward Johnson for their excellent support during the experiment. Thanks also to the ARL:UT dive team: Dave Gage, Roger Banks and Tim Josserand. Lastly, the authors thank Robert Headrick and Office of Naval Research, Ocean Acoustics for support and encouragement.

References

[1] M. Isakson, J. Piper, N. Chotiros, and H. Camin, "Acoustic reflection and transmission experiments from 4.5 to 50 kHz at the Sediment Acoustics EXperiment SAX04", in *Proceedings of the 1st International Conference "Underwater Acoustic Measurements: Technologies and Results"*, edited by J. Papadakis and L. Bjorno, 309–316 (F.O.R.T.H., Crete) (2005).

[2] H. Camin and M. Isakson, "A comparison of spherical wave sediment reflection coefficient measurements to elastic and poro-elastic models", Journal of the Acoustical Society of America **120**, 2437–2449 (2005).

[3] K. Briggs and A. Reed, "Using CT to image storn-generated stratigraphy in sandy sediment off Fort Walton Beach, Florida, USA", in *Proceedings of the 1st International Conference "Underwater Acoustic Measurements: Technologies and Results"*, edited by J. Papadakis and L. Bjorno, 95–102 (F.O.R.T.H., Crete) (2005).

[4] W. Press, S. Teukolsky, W. Vetterling, and B. Flannery, *Numerical Recipes, 2nd Ed., Chapter 14* (Cambridge University Press, Cambridge) (1992).

[5] H. Schmidt, *OASES Version 2.1 User Guide and Reference Manual, Chapter 8* (Department of Ocean Engineering, Massachusetts Institute of Technology, Cambridge) (1997).

[6] D. Tang, B. Hefner, K. Briggs, A. Reed, K. WIlliams, and E. Thorsos, "Measurements of sediment interface and subbottom properties", in *Proceedings of the 1st International Conference "Underwater Acoustic Measurements: Technologies and Results"*, edited by J. Papadakis and L. Bjorno, 293–300 (F.O.R.T.H., Crete) (2005).

[7] E. Thorsos, "The validity of the Kirchoff approximation for rough surface scattering using a Gaussian roughness spectrum", Journal of the Acoustical Society of America **83**, 78–92 (1988).

[8] M. Isakson, R. Yarbrough, and N. Chotiros, "A finite element model for seafloor roughness scattering", in *Proceedings of the International Symposium on Underwater Reverberation and Clutter*, 173–180 (N.U.R.C., La Spezia, Italy) (2008).

[9] M. Zampolli, A. Tesei, and F. Jensen, "A computationally efficient finite element model with perfectly matched layers applied to scattering from axially symmetric objects", Journal of the Acoustical Society of America **122**, 1472–1485 (2007).

[10] K. Williams, D. Jackson, E. Thorsos, D. Tang, and S. Schock, "Comparison of sound speed and attenuation measured in a sandy sediment to predictions based on the Biot theory of porous media", IEEE Journal of Ocean Engineering **27**, 413–428 (2002).

[11] M. Biot, "Theory of propagation of elastic waves in a fluid saturated porous solid I. Low frequency range", Journal of the Acoustical Society of America **28**, 168–178 (1956).

[12] M. Biot, "Theory of propagation of elastic waves in a fluid saturated porous solid II. Higher frequency range", Journal of the Acoustical Society of America **28**, 179–191

(1956).

[13] R. Stoll, *Sediment Acoustics, Lecture Notes in Earth Science*, chapter 1 (Springer Verlag) (1983).

[14] N. Chotiros and M. Isakson, "Acoustic virtual mass of granular media", Journal of the Acoustical Society of America **121**, EL70–EL76 (2007).

[15] R. Stoll, "Velocity dispersion in water-saturated granular sediment", Journal of the Acoustical Society of America **111**, 785–793 (2002).

[16] M. Buckingham, "Wave propagation, stress relaxation, and grain-to-grain shearing in saturated, unconsolidated marine sediments", Journal of the Acoustical Society of America **108**, 2796–2815 (2000).

[17] D. Jackson and M. Richardson, *High-frequency seafloor acoustics, Appendix B*, Underwater Acoustics (Springer Verlag) (2007).

[18] M. Richardson, K. Briggs, A. Reed, W. Vaughan, M. Zimmer, and R. Ray, "Characterization of the environment during SAX04: Preliminary results", in *Proceedings of the 1st International Conference "Underwater Acoustic Measurements: Technologies and Results"*, edited by J. Papadakis and L. Bjorno, 285–292 (F.O.R.T.H., Crete) (2005).

[19] K. Briggs, M. Zimmer, and M. Richardson, "Spatial and temporal variations in sediment compressional wave speed and attenuation measured at 400 khz for SAX04", in *Boundary influences in high frequency, shallow water acoustics*, edited by N. Pace and P. Blondel, 29–37 (University of Bath Press, Bath, England) (2005).

[20] R. Wheatcroft, "Biogenic ripple destruction: rates, modes and subsurface consequences", Proc. SAX04 workshop, 21 March (2007).

[21] E. Hamilton, "Geoacoustic modeling of the sea floor", Journal of the Acoustical Society of America **68**, 1313–1340 (1980).

TABLE I. Number of pings used to average replica data

Receiver	4.5 - 10 kHz	10 - 22 kHz	22 - 50 kHz
Lowest Receiver	7	10	97
Mid Receiver	10	166	218
Highest Receiver	101	218	520

TABLE II. Model parameters

Parameter/Sediment Type	Water	Sand	Mud	"Gassy" Sediment
Density- g/cm^3	1.026	2.041	1.524	0.51
Compressional Sound Speed - m/s	1529	1772	1546	760
Compressional Attenuation - dB/m/kHz	0.0001	0.25	0.1	0.25

List of Figures

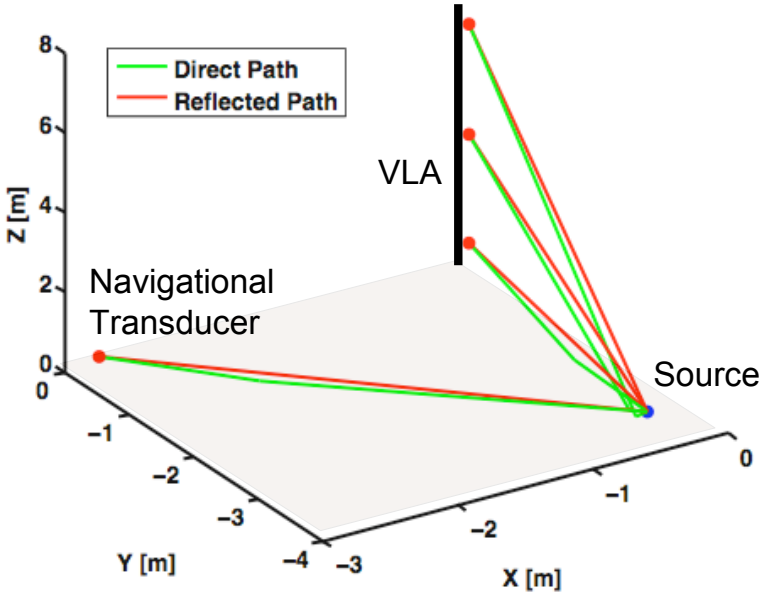

FIG. 1. Perspective view of the experiment. Localization of the vehicle was performed by calculating the distance to each receiver from the arrival of the direct path. The overdetermined system allowed the exclusion of data in which the water column was significantly perturbed.

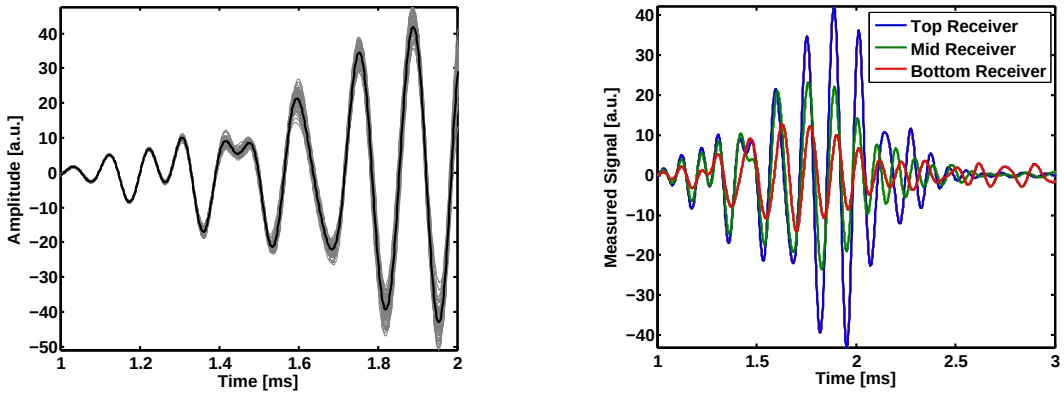

(a) (b)

FIG. 2. In situ replicas were determined by aligning the first arrival of the direct path and averaging over pings which had different reflected path arrivals. Alignment and averaging for the low frequency chirp are shown in (a). The dark line indicates the average while the lighter gray lines indicate individual measurements. The replicas for this chirp determined for each receiver are shown in (b).

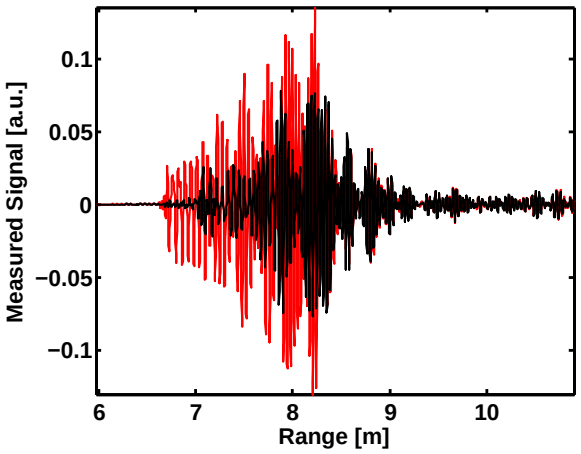

(a)

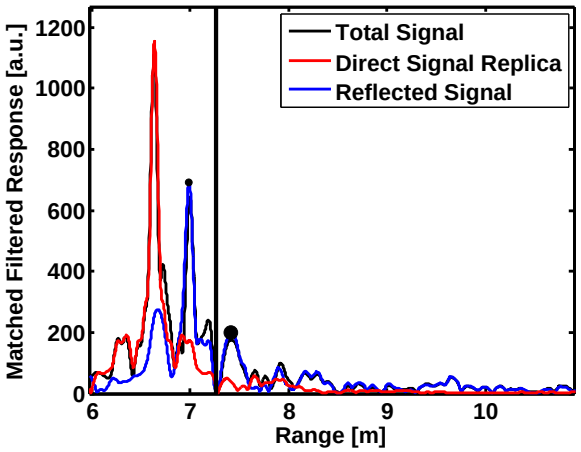

(b)

FIG. 3. Replicas such as those shown in Fig. 2 were aligned and subtracted from each ping. Shown in (a) is an example of the direct path subtraction from the raw data. The absolute value of the matched filter response of both the raw data and direct path subtracted data is shown in (b). Two reflectors are measured indicated by solid black circles. The expected arrival of the reflected path from a flat surface is indicated by the solid dark line.

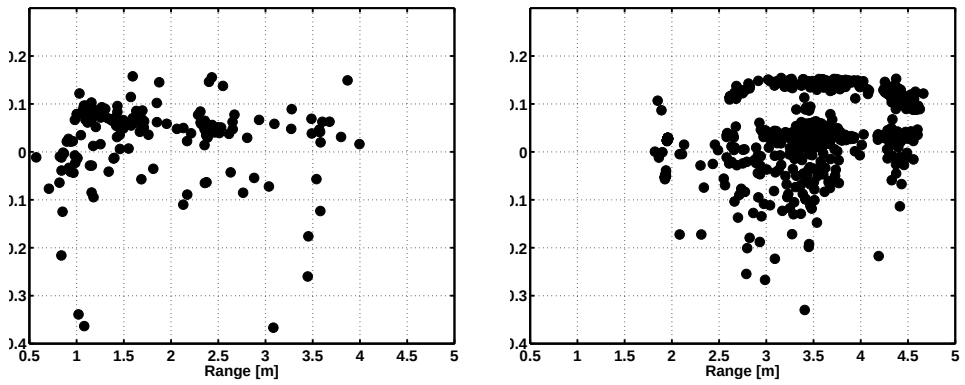

(a) (b)

FIG. 4. Calculated depths of reflectors based on the source/receiver geometry and arrival time as a function of range. Shown in (a) are depths from the signal centered at 16 kHz. In (b) are the depths from the 36 kHz pulse.

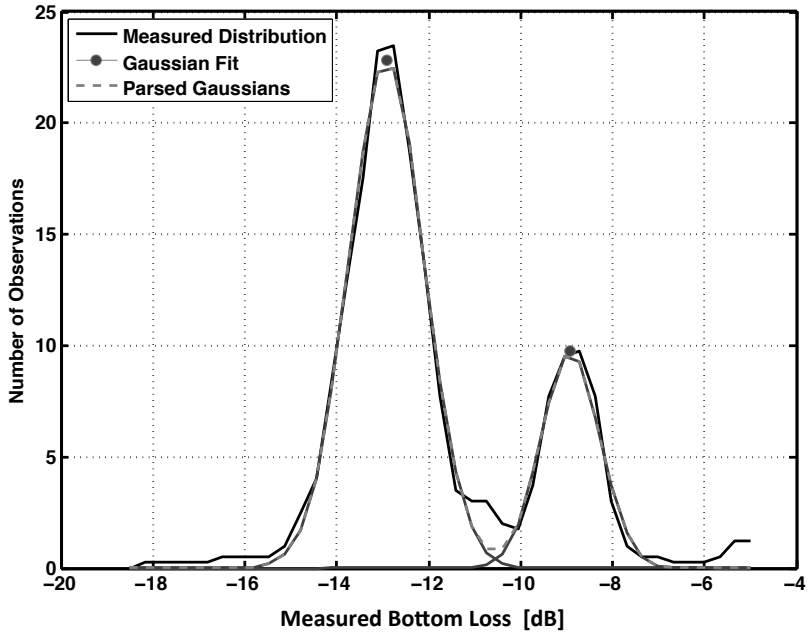

FIG. 5. The data distribution from 68 degrees grazing at 36 kHz parsed into component Gaussians.

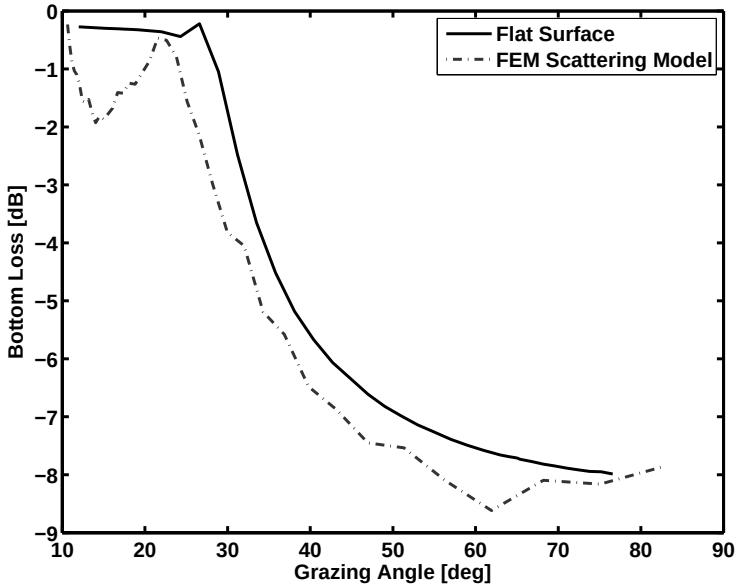

FIG. 6. Bottom loss for a flat surface compared with loss from a rough interface based on the measured spectrum.

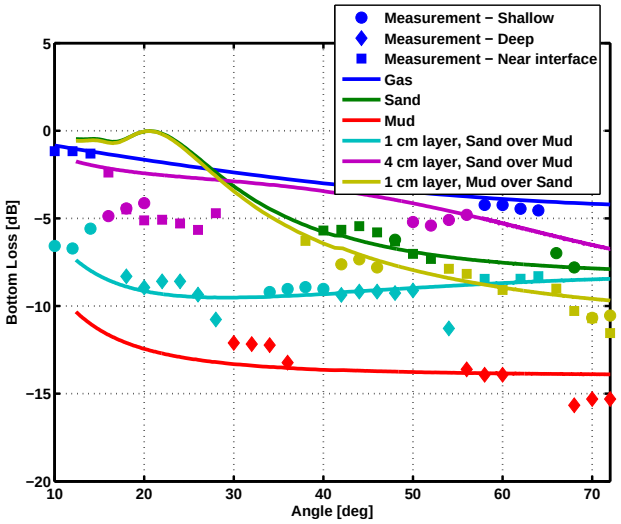

(a)

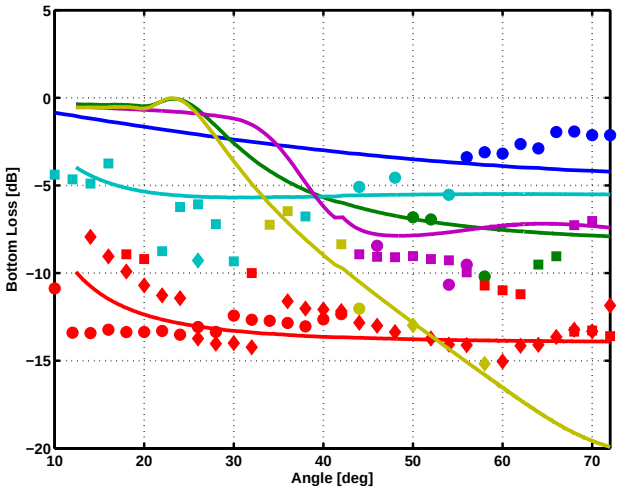

(b)

FIG. 7. Bottom loss measurements compared with layered models based on the parameters given in Table II. Error bars are not included for clarity. The lower frequency results centered at 16 kHz are shown in (a) while the higher frequency results centered at 36 kHz are shown in (b).

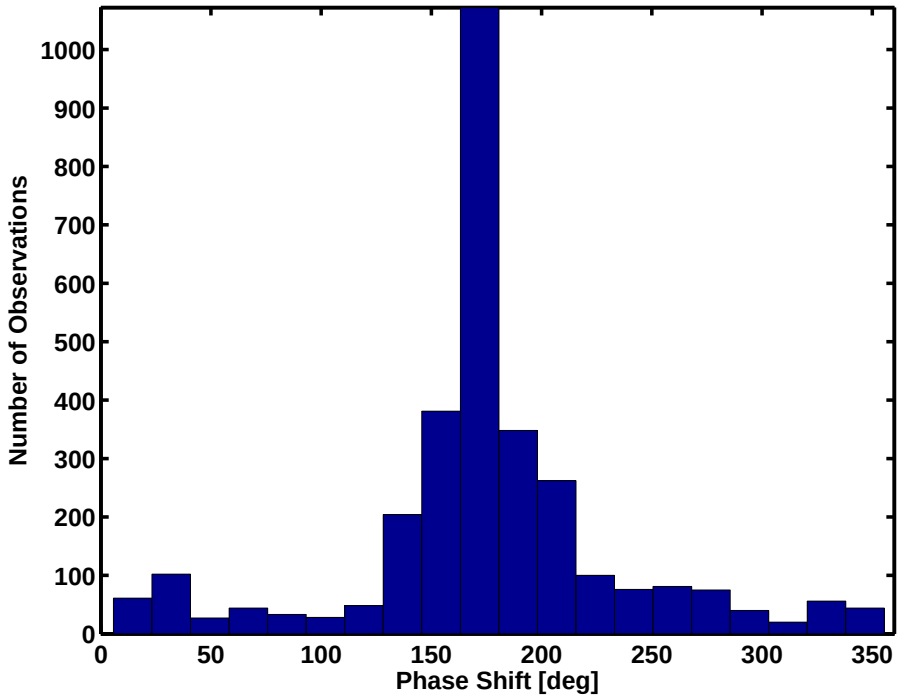

FIG. 8. Measured phase for reflections from 22 to 50 kHz that are greater than -6 dB and between 40 and 80 degrees grazing. The 180 degree phase shift indicates a reflection from a pressure release such as a very gassy sediment or fish.